

Investigating High Mass X-ray Binaries at hard X-rays with INTEGRAL

Lara Sidoli  and Adamantia Paizis

INAF/IASF Milano, Istituto di Astrofisica e Fisica Cosmica di Milano
via A. Corti 12, I-20133, Milano, Italy
emails: lara.sidoli@inaf.it, adamantia.paizis@inaf.it

Abstract. The *INTEGRAL* archive developed at INAF-IASF Milano with the available public observations from late 2002 to 2016 is investigated to extract the X-ray properties of 58 High Mass X-ray Binaries (HMXBs). This sample consists of sources hosting either a Be star (Be/XRBs) or an early-type supergiant companion (SgHMXBs), including the Supergiant Fast X-ray Transients (SFXTs). *INTEGRAL* light curves (sampled at 2 ks) are used to build their hard X-ray luminosity distributions, returning the source duty cycles, the range of variability of the X-ray luminosity and the time spent in each luminosity state. The phenomenology observed with *INTEGRAL*, together with the source variability at soft X-rays taken from the literature, allows us to obtain a quantitative overview of the main sub-classes of massive binaries in accretion (Be/XRBs, SgHMXBs and SFXTs). Although some criteria can be derived to distinguish them, some SgHMXBs exist with intermediate properties, bridging together persistent SgHMXBs and SFXTs.

Keywords. X-rays: binaries, accretion

1. Introduction

High Mass X-ray Binaries (HMXBs) host a compact object (most frequently a neutron star [hereafter, NS]) accreting matter from an O or B-type massive star. In the great majority of these systems the mass transfer to the accretor occurs by means of the stellar wind, while in a limited number of HMXBs (SMC X-1, LMC X-4, Cen X-3) it happens through Roche Lobe overflow (RLO). Before the launch of the *INTEGRAL* satellite (Winkler *et al.* 2003, Winkler *et al.* 2011), two types of HMXBs were known, depending on the kind of companion, either an early type supergiant star (SgHMXBs) or a Be star (Be/XRBs).

Nowadays the scenario has significantly changed, with a number of Galactic HMXBs tripled and new sub-classes of massive binaries (the “highly obscured sources” and the “Supergiant Fast X-ray Transients”, SFXTs) discovered thanks to the observations of the Galactic plane performed by the *INTEGRAL* satellite. The first type includes HMXBs where the absorbing column density due to the local matter is more than one order of magnitude larger than the average in HMXBs (reaching 10^{24} cm⁻² in IGR J16318–4848).

The SFXTs are HMXBs that undergo short (usually less than a few days) outbursts made of brief (typical duration of ~ 2 ks) and bright X-ray flares (peak $L_X \sim 10^{36}$ erg s⁻¹), while most of their time is spent below $L_X \sim 10^{34}$ erg s⁻¹. The physical mechanism producing this behavior is debated: the main models involve different ways to prevent accretion onto the NS (invoking opposite assumptions on the NS magnetic field and spin period), coupled with different assumptions on the donor (clumpy and/or magnetized) wind parameters (see Martínez-Núñez *et al.* 2017, Walter *et al.* 2015 and Sidoli 2017 for recent reviews, and references therein).

While SgHMXBs and Be/XRBs differ in the type of their companion star, the boundaries between SgHMXBs and SFXTs are based *only* on their X-ray phenomenology (persistent vs transient X-ray emission), since they both harbour an early-type supergiant donor. In fact, unlike SgHMXBs, SFXTs display a large dynamic range that can reach six orders of magnitude in X-ray luminosity, between quiescence and the outburst peak (as in IGR J17544-2619; in't Zand (2005), Romano *et al.* (2015)). For other SFXTs the range of flux variability is typically comprised between 10^2 and 10^4 .

The present *paper* summarizes our systematic analysis of the *INTEGRAL* observations of HMXBs, spanning fourteen years of operations, from 2002 to 2016. The main aim of this work is to obtain an overall, quantitative, characterization of the different sub-classes of HMXBs at hard X-rays (above 18 keV) and to put this phenomenology into context of other known properties (like pulsar spin period, orbital geometry) and soft X-ray behavior (1–10 keV), as described in the literature. We refer the reader to Sidoli & Paizis (2018) for more details on this work.

2. The *INTEGRAL* archive and the selection of the sample

Our investigation is based on observations performed by IBIS/ISGRI on-board the *INTEGRAL* satellite and it is focussed on the energy range 18–50 keV. We built an *INTEGRAL* local archive of all public observations (see Paizis *et al.* 2013 and Paizis *et al.* 2016 for the technical details). For all known HMXBs we extracted the long-term light curves of the sources (bin time of ~ 2 ks, the typical duration of an *INTEGRAL* observation, called “Science Window”) spanning fourteen years (from late 2002 to 2016). We retained in our final sample only the sources which were detected (above 5 sigma) in at least one *INTEGRAL* observation (i.e. one single Science Window), within 12° from the centre of the field-of-view. These selection criteria translated into a sensitivity threshold of a few 10^{-10} erg cm $^{-2}$ s $^{-1}$ (18–50 keV) for our survey, and into a total exposure time of ~ 200 Ms for the final HMXB sample.

The final list of sources includes 58 HMXBs, classified in the literature as SgHMXBs (18 sources), SFXTs (13 sources) and Be/XRBs (20 sources); the remaining 9 massive binaries are two pulsars accreting from early type giant stars (LMC X-4 and Cen X-3), three black hole (candidate) systems (Cyg X-1, Cyg X-3, SS 433) plus two peculiar massive binaries (IGR J16318-4848 and 3A 2206+543). Then, we also included a symbiotic binary XTE J1743-363, that is a different kind of wind-fed system, to compare it with massive binaries. The complete list of sources is reported in Table 1, together with their sub-class, as reported in the literature.

3. *INTEGRAL* results

Duty Cycles (18-50 keV). The long-term light curves for our sample of HMXBs were used to calculate the source duty cycle in the energy range 18-50 keV ($DC_{18-50 \text{ keV}}$), defined as the percentage of detections (at ~ 2 ks time bin) or, in other words, the ratio between the exposure time when the source is detected and the total exposure time at the source position. Table 1 (third column) lists the values obtained. Even in case of a persistent SgHMXB, the duty cycle can be lower than 100%, because of source variability leading the source flux below the IBIS/ISGRI threshold of detectability on the adopted time bin. Eclipses or off-states also reduce the source duty cycle in persistent sources (e.g. in Vela X-1, Kreykenbohm *et al.* 2008; Sidoli *et al.* 2015). The advantage of the adoption of a long-term archive, analysed here in a systematic way, is that we are confident that the source duty cycles are close to the real source activity, above the *INTEGRAL* sensitivity. We refer the reader to Sidoli & Paizis (2018) for a detailed discussion of the possible observational biases.

Table 1. Results of our survey of a sample of HMXBs.

Source	sub-class	DC _{18–50keV} [%]	Av. Luminosity (18–50 keV) ¹ [erg s ⁻¹]	DR _{1–10keV} (F _{max} /F _{min})
SMC X-1	SgHMXB	49.05	1.7E+38	7.7
3A 0114+650	SgHMXB	14.63	2.1E+36	–
Vela X-1	SgHMXB	79.22	1.3E+36	1.7
1E 1145.1-6141	SgHMXB	31.95	3.0E+36	–
GX 301-2	SgHMXB	94.47	2.8E+36	2.6
H 1538-522	SgHMXB	30.15	9.2E+35	32.9
IGR J16207-5129	SgHMXB	0.39	1.1E+36	9.3
IGR J16320-4751	SgHMXB	21.32	5.9E+35	14.7
IGR J16393-4643	SgHMXB	0.40	3.4E+36	3.2
OA0 1657-415	SgHMXB	59.78	5.8E+36	10.0
4U 1700-377	SgHMXB	73.09	1.1E+36	12.0
IGR J17252-3616	SgHMXB	4.65	2.9E+36	17.3
IGR J18027-2016	SgHMXB	0.54	5.2E+36	375
IGR J18214-1318	SgHMXB	0.06	3.4E+36	–
XTE J1855-026	SgHMXB	9.64	4.2E+36	–
H 1907+097	SgHMXB	20.13	8.1E+35	546
4U 1909+07	SgHMXB	24.84	7.1E+35	11.5
IGR J19140+0951	SgHMXB	14.18	5.2E+35	769
LMC X-4	giant HMXB	47.23	1.2E+38	3.4
Cen X-3	giant HMXB	62.79	4.0E+36	5.0
IGR J08408-4503	SFXT	0.09	3.0E+35	6750
IGR J11215-5952	SFXT	0.64	1.6E+36	>480
IGR J16328-4726	SFXT	0.28	1.7E+36	300
IGR J16418-4532	SFXT	1.22	6.1E+36	308
IGR J16465-4507	SFXT	0.18	2.9E+36	37.5
IGR J16479-4514	SFXT	3.33	3.6E+35	1667
IGR J17354-3255	SFXT	0.01	3.0E+36	>929
XTE J1739-302	SFXT	0.89	4.8E+35	>2040
IGR J17544-2619	SFXT	0.54	5.6E+35	1.67×10 ⁶
SAX J1818.6-1703	SFXT	0.81	2.9E+35	>1364
IGR J18410-0535	SFXT	0.53	3.8E+35	1.1×10 ⁴
IGR J18450-0435	SFXT	0.35	1.5E+36	513
IGR J18483-0311	SFXT	4.63	5.2E+35	899
H 0115+634	Be/XRB	9.55	1.5E+37	1.4×10 ⁵
RX J0146.9+6121	Be/XRB	0.11	1.1E+35	–
EXO 0331+530	Be/XRB	25.10	2.4E+37	1.07×10 ⁶
X Per	Be/XRB	76.96	2.5E+34	10
1A 0535+262	Be/XRB	12.34	4.4E+36	2.7×10 ⁴
GRO J1008-57	Be/XRB	8.87	2.4E+36	181
4U 1036-56	Be/XRB	0.35	7.5E+35	60
IGR J11305-6256	Be/XRB	0.41	1.9E+35	–
IGR J11435-6109	Be/XRB	2.68	1.4E+36	–
H 1145-619	Be/XRB	1.07	1.2E+35	250
XTE J1543-568	Be/XRB	0.14	2.7E+36	8
AX J1749.1-2733	Be/XRB	0.17	8.1E+36	–
GRO J1750-27	Be/XRB	4.88	2.9E+37	>10
AX J1820.5-1434	Be/XRB	0.15	2.1E+36	–
Ginga 1843+009	Be/XRB	3.39	5.8E+36	5660
XTE J1858+034	Be/XRB	5.34	8.8E+36	–
4U 1901+03	Be/XRB	10.44	1.2E+37	1000
KS 1947+300	Be/XRB	9.41	6.8E+36	800
EXO 2030+375	Be/XRB	28.99	7.8E+36	>2784
SAX J2103.5+4545	Be/XRB	11.14	2.0E+36	6364
IGR J16318-4848	other HMXB	35.17	7.4E+35	3.3
3A 2206+543	other HMXB	6.41	2.5E+35	250
Cyg X-1	other HMXB	99.88	2.5E+36	3.7
Cyg X-3	other HMXB	93.49	1.0E+37	4.9
SS 433	other HMXB	14.97	8.5E+35	5.0
XTE J1743-363	symbiotic	0.13	1.1E+36	6.2

Notes: ¹This 18–50 keV luminosity is an average over *INTEGRAL* detections only. This implies that, for transients, it is an average luminosity in outburst. See Sidoli & Paizis (2018) for the source distances adopted here.

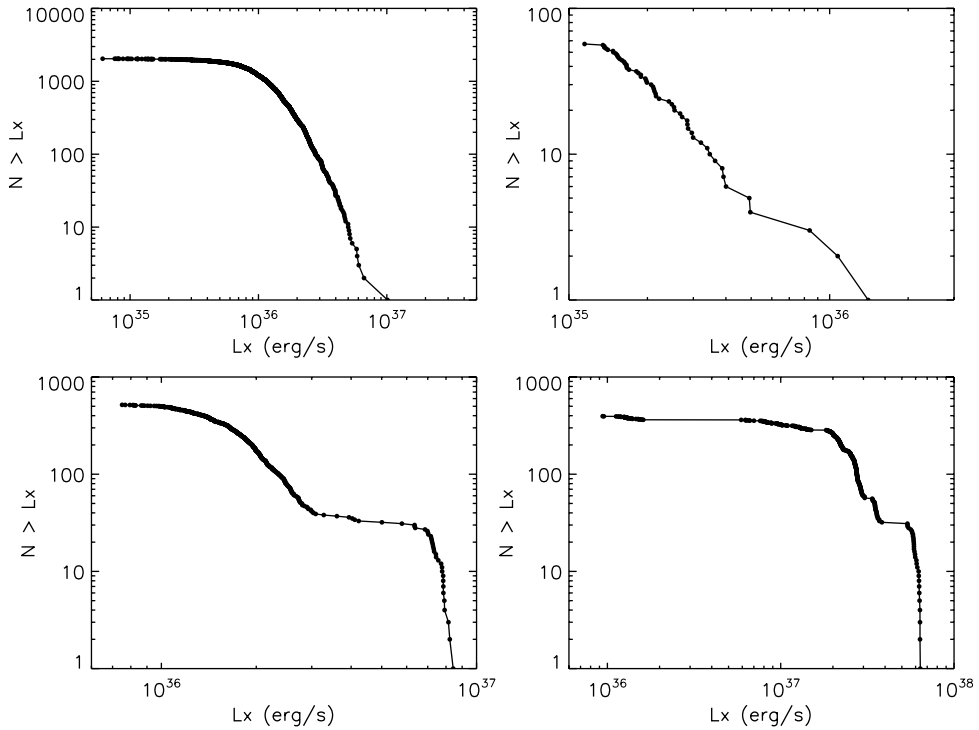


Figure 1. CLDs of sources representative of the three sub-classes of HMXBs: from left to right, from top to bottom, the persistent SgHMXB Vela X-1, the SFXT SAX J1818.6-1703 and the two Be transients SAX J2103.5+4545 and EXO 0331+530.

Cumulative Luminosity Distributions. The hard X-ray light curves were used to extract the Cumulative Luminosity Distributions (CLDs). We adopted a single average conversion factor of 4.5×10^{-11} erg cm $^{-2}$ count $^{-1}$ from IBIS/ISGRI count-rates to X-ray fluxes (18–50 keV) and assumed the source distances reported by Sidoli & Paizis (2018).

The CLDs of four sources are shown in Fig. 1, representative of the behavior of a persistent SgHMXB (Vela X-1), a SFXT (SAX J1818.6-1703) and of two transient Be/XRBs (SAX J2103.5+4545 and EXO 0331+530). Their shape appears different: a lognormal-like distribution is evident in Vela X-1, a powerlaw CLD in the SFXT, while a more complex behavior is present in the Be/X-ray transients.

Since the timescale of the SFXT flare duration is similar to the bin time of the *INTEGRAL* light curves, the SFXT CLDs are distributions of the SFXT flare luminosities (Paizis & Sidoli 2014). The difference among supergiant systems (SgHMXBs vs SFXTs), between lognormal and powerlaw-like luminosity distributions were already found by Paizis & Sidoli (2014) from the analysis of the first nine years of *INTEGRAL* observations of a sample of SFXTs, compared with three SgHMXBs.

This behavior might be ascribed to a separate physical mechanism producing the bright X-ray flares in SFXTs: in the framework of the quasi-spherical settling accretion regime (Shakura *et al.* 2012), hot wind matter, captured within the Bondi radius, accumulates above the NS magnetosphere; magnetic reconnection at the base of this shell (between the magnetized, captured, wind matter and the NS magnetosphere) has been suggested to enhance the plasma entry through the magnetosphere, opening the NS gate. This allows the sudden accretion of the shell material onto the NS and the emission of the SFXT flares (Shakura *et al.* 2014). The detection of a \sim kG magnetic field from the companion of the SFXT IGR J11215–5952 supports this scenario (Hubrig *et al.* 2018).

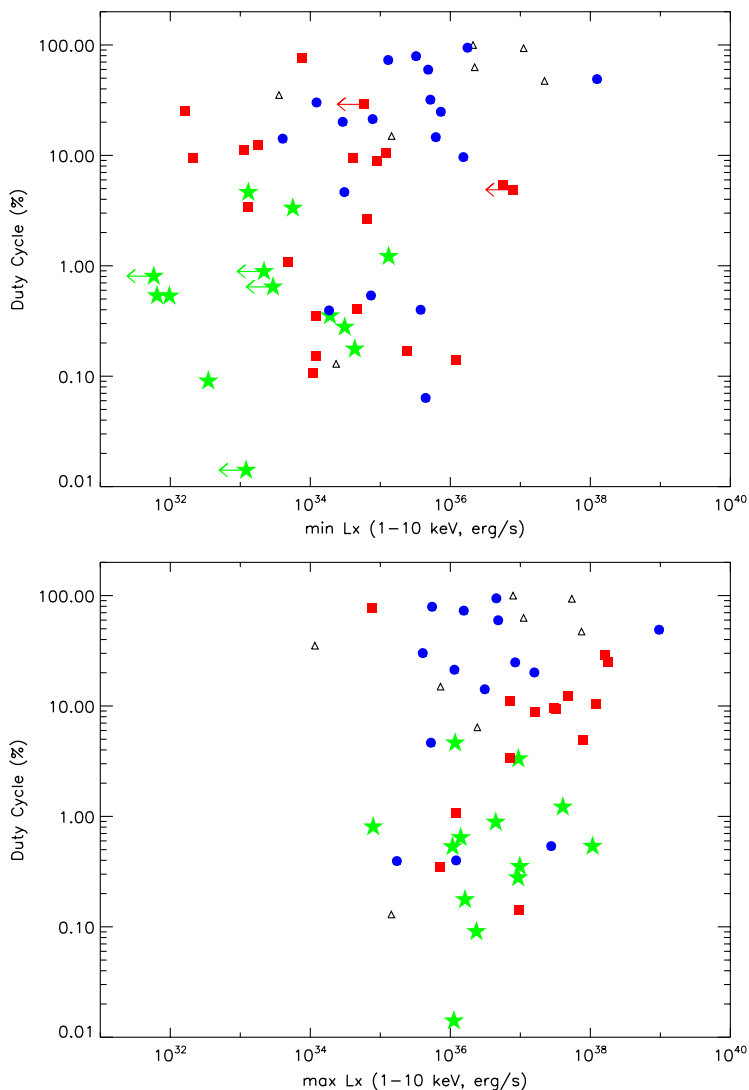


Figure 2. *INTEGRAL* source duty cycle ($DC_{18-50\text{ keV}}$) versus the soft X-ray luminosities reported in the literature (minimum and maximum ones are in the upper and lower panels, respectively). Symbols indicate four sub-classes: blue circles for SgHMXBs, green stars for SFXTs, red squares for Be/XRBs and empty thin diamonds for the remaining types of sources, as reported in Table 1 (the “other” HMXBs, together with the two giant HMXBs and the symbiotic system). Arrows indicate upper limits on the minimum flux. Note that the different number of sources reported in the two panels are because for some HMXBs we have found in the literature only a single value for the soft X-ray flux (and we ascribed it to the “minimum 1-10 keV flux”).

Transient Be/XRBs can show two types of outbursts, the “normal” and the “giant” ones (Stella *et al.* 1986; Negueruela *et al.* 1998, 2001,b; Okazaki *et al.* 2001; Reig 2011; Kuhnel *et al.* 2015). The first type happens periodically and is produced by the higher accretion rate when the NS approaches the decretion disc of the Be star, at each passage near periastron. The second type of outburst can occur at any orbital phase, is more luminous than the normal one and is thought to be produced by major changes in the Be decretion disc structure. We ascribe the bimodal behaviour evident in the CLD of

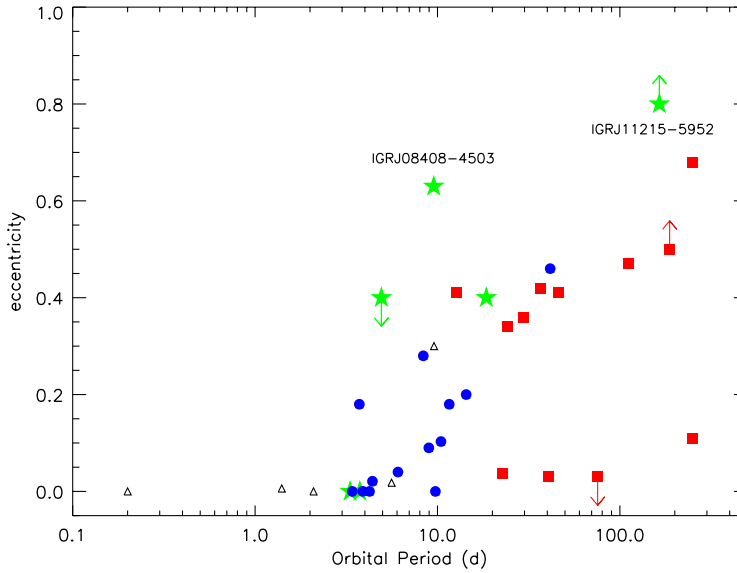


Figure 3. Orbital eccentricity versus orbital period for our sample of HMXBs. The symbols have the same meaning as in Fig. 2.

SAX J2103.5+4545 shown in Fig. 1 to the two different luminosities reached during the two types of outbursts: low (high) luminosity in normal (giant) one, respectively. Other Be/XRBs show more complex shapes, multi-modal distributions (like in the case of EXO 0331+530 shown in Fig. 1), indicative of multi peaks within the same outburst, or outbursts reaching different peak luminosities.

The CLDs of all HMXBs of our sample are reported by Sidoli & Paizis (2018; their Fig. 1-4). In their normalized version, these functions allow the reader to obtain in one go, not only an easy comparison between all kind of HMXBs, but also to quantify the time spent by each HMXB in any given luminosity state, above the instrumental sensitivity.

Average Luminosity (18-50 keV). An average luminosity (18-50 keV) was calculated for each source, over the *INTEGRAL* detections (at 2 ks timescale; see Table 1, forth column). Note that this definition implies that, for transient sources, this is an average luminosity *in outburst*.

4. Other HMXB properties from the literature

Dynamic Ranges (1-10 keV). Other source properties were collected from the literature, in order to put the *INTEGRAL* behavior into a wider context: distance, pulsar spin and orbital period, eccentricity of the orbit, maximum and minimum fluxes in soft X-rays (1–10 keV, corrected for the absorption). These latter were investigated since the instruments observing the sky at soft X-rays are much more sensitive than *INTEGRAL* and can probe the true quiescent state in transient sources, together with their variability range between quiescence and outburst peak.

When the published soft X-ray fluxes were not available in the 1–10 keV range, we extrapolated them using *WEBPIMMS* and the appropriate model found in the literature. Then, we calculated their ratio (the dynamic range “ $DR_{1-10\text{ keV}} = F_{max} / F_{min}$ ”, reported in Table 1, last column). When only a single value for the soft X-ray flux was found, the dynamic range was not calculated (“–” in Table 1) and the flux was ascribed to the “minimum flux”. Note that we considered only spin-phase-averaged fluxes for X-ray pulsars, and out-of-eclipse minimum fluxes for eclipsing systems, to obtain the intrinsic range of X-ray variability.

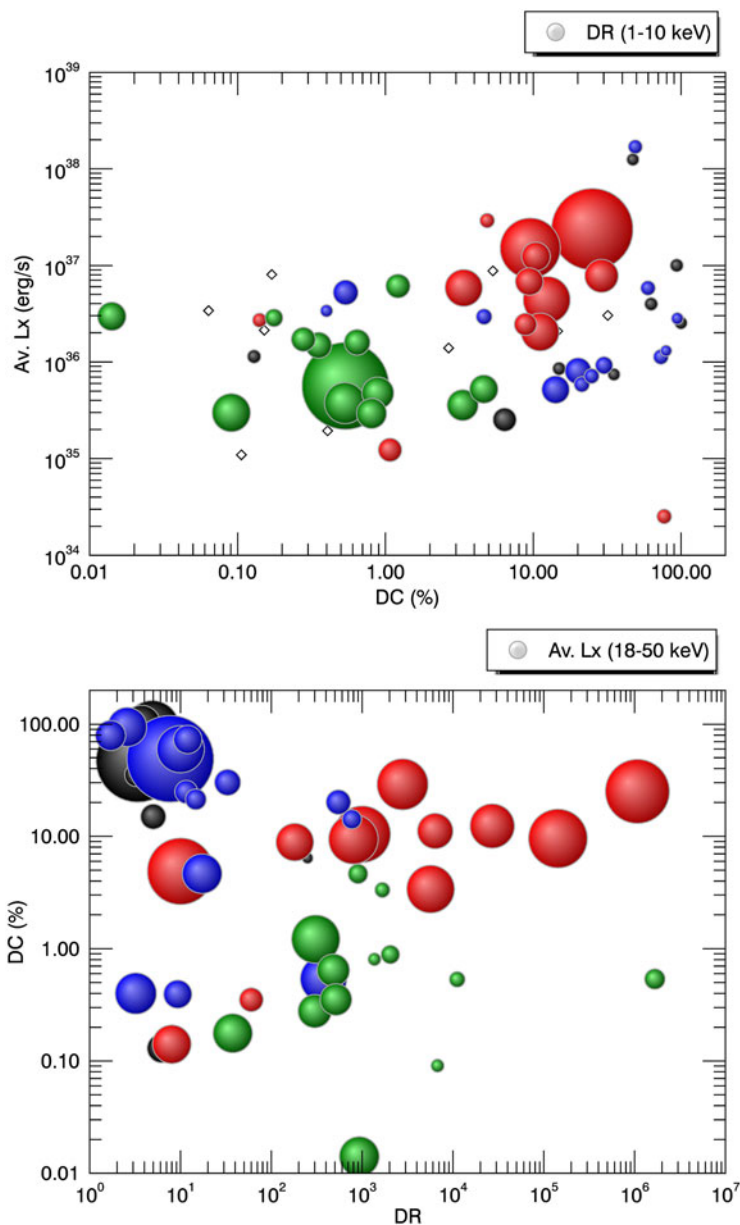


Figure 4. Bubbleplots summarizing the results obtained, focussing on three main quantities: $DC_{18-50\text{ keV}}$, $DR_{1-10\text{ keV}}$ and the average luminosity in the energy range 18–50 keV (note that, for transient sources, this is a luminosity during outburst, as observed by *INTEGRAL*). *Upper panel:* average $L_{18-50\text{ keV}}$ vs $DC_{18-50\text{ keV}}$; each bubble indicates a single source, with the bubble size correlating with the $DR_{1-10\text{ keV}}$. The diamonds mark the position of sources for which the $DR_{1-10\text{ keV}}$ could not be calculated (only a single flux in the 1-10 keV energy band was found in the literature). In blue we mark the SgHMXBs, in red the Be/XRBs and in green the SFXTs. In black, all other systems are indicated (the “other” HMXBs reported in Table 1, together with the giant HMXBs and the symbiotic binary). *Lower panel:* $DC_{18-50\text{ keV}}$ vs $DR_{1-10\text{ keV}}$, with bubble sizes correlating with the average $L_{18-50\text{ keV}}$.

In Fig. 2 we show the source $DC_{18-50 \text{ keV}}$ plotted against the minimum and maximum luminosities (1–10 keV), for different HMXB sub-classes: the scatter is huge in the upper panel where the duty cycle is plotted versus the minimum soft X-ray luminosity. The SFXTs are located in the lower left part of the plot, at low $DC_{18-50 \text{ keV}}$ and X-ray luminosity in quiescence, while the persistent SgHMXB mostly lie in the upper right part, at both high luminosities and large duty cycles. Be/XRBs appear located in-between them. In the lower panel, where the maximum soft X-ray luminosity is considered, the sub-classes regroup to the right, at more similar luminosities (in outbursts for SFXTs and Be/X-ray transients). A few sources, classified in the literature as SgHMXB (blue circles in Fig. 2), display a very low $DC_{18-50 \text{ keV}}$, similar to SFXTs. They might be either mis-classified transients or persistent sources emitting X-rays at a level just below the instrumental sensitivity, that are detected only during sporadic flaring. Note that the HMXBs almost reaching the Eddington luminosity are the RLO systems SMC X-1 and LMC X-4.

Orbital geometry. Among the many trends of source properties we have investigated for our sample (see Sidoli & Paizis, 2018), we report here on the plot showing the system eccentricity versus the orbital period (Fig. 3). Two trends are evident, above $P_{orb} \sim 10$ d: low eccentricity Be/XRBs with no correlation with the orbital period (X Per is the prototype) and a group of binaries (mostly Be/XRBs) where the eccentricity correlates with the orbital period. SgHMXBs are located at lower eccentricities and orbital periods. This plot has already been investigated in the literature (Townsend *et al.* 2011). The novelty here is the inclusion of SFXTs (not considered by Townsend *et al.* 2011): some of them display circular orbits, while others very eccentric geometries, like IGR J08408-4503 ($e=0.63$ and $P_{orb}=9.54$ d) and IGR J11215-5952 ($e > 0.8$ and $P_{orb}=165$ d). These SFXTs enable the HMXBs hosting supergiant stars to extend at larger eccentricities and orbital periods, in a parameter space that is unusual even for Be/XRBs.

5. Conclusions

We summarize the results of our systematic analysis in Fig. 4, making use of three characterizing quantities: two of them have been derived from the analysis of fourteen years of INTEGRAL observations ($DC_{18-50 \text{ keV}}$ and the average 18–50 keV luminosity, in outburst for transients), while the third one has been calculated from soft X-ray fluxes taken (or extrapolated) from the literature ($DR_{1-10 \text{ keV}}$).

We have obtained a global view of a large number of HMXBs where the different kind of sources tend to cluster mainly in different region of this 3D space, as follows:

- SgHMXBs (excluding the high luminosity RLO systems) in general show low $DR_{1-10 \text{ keV}}$ (< 40), high duty cycles ($DC_{18-50 \text{ keV}} > 10$ per cent), low average 18–50 keV luminosity ($\sim 10^{36} \text{ erg s}^{-1}$);
- SFXTs are characterized by high $DR_{1-10 \text{ keV}}$ (> 100), low duty cycles ($DC_{18-50 \text{ keV}} < 5$ per cent), low average 18–50 keV luminosity in outburst ($\sim 10^{36} \text{ erg s}^{-1}$);
- Be/XRTs display a high $DR_{1-10 \text{ keV}}$ (> 100), intermediate duty cycles ($DC_{18-50 \text{ keV}} \sim 10$ per cent), high average 18–50 keV luminosity in outburst ($\sim 10^{37} \text{ erg s}^{-1}$).

It is worth mentioning that a number of HMXBs exist that displays intermediate properties, in particular among SgHMXB, sometimes overlapping with some region of the parameter space more typical of SFXTs, bridging together the two sub-classes. This seems to indicate that these two sub-classes have no sharp boundaries, but their phenomenology is based on continuous parameters, from persistent SgHMXBs towards the most extreme SFXT (IGR J17544-2619).

References

- Hubrig S., Sidoli L., Postnov K., Schöller M., Kholtygin A. F., Järvinen S. P., & Steinbrunner P., 2018, *MNRAS*, 474, L27
- in't Zand J. J. M., 2005, *A&A*, 441, L1
- Kreykenbohm I., Wilms J., Kretschmar P., Torrejón J. M., Pottschmidt K., Hanke M., Santangelo A., Ferrigno C., & Staubert R., 2008, *A&A*, 492, 511
- Kuehnel M., Kretschmar P., Nespoli E., Okazaki A. T., Schoenherr G., Wilson-Hodge C. A., Falkner S., Brand T., Anders F., Schwarm F.-W., Kreykenbohm I., Mueller S., Pottschmidt K., Fuerst F., Grinberg V., & Wilms J., 2015, in Proceedings of "A Synergistic View of the High Energy Sky" - 10th INTEGRAL Workshop (INTEGRAL 2014). 15-19 September 2014. Annapolis, MD, USA. Published online at <http://pos.sissa.it/cgi-bin/reader/conf.cgi?confid=228> The Be X-ray Binary Outburst Zoo II. p. 78
- Martínez-Núñez S., Kretschmar P., Bozzo E., Oskinova L. M., Puls J., Sidoli L., Sundqvist J. O., Blay P., *et al.* 2017, *Space Science Reviews*, 212, Issue 1-2, 59
- Negueruela I., Reig P., Coe M. J., & Fabregat J., 1998, *A&A*, 336, 251
- Negueruela I., & Okazaki A. T., 2001, *A&A*, 369, 108
- Negueruela I., Okazaki A. T., Fabregat J., Coe M. J., Munari U., & Tomov T., 2001, *A&A*, 369, 117
- Okazaki A. T., & Negueruela I., 2001, *A&A*, 377, 161
- Paizis A., Mereghetti S., Götz D., Fiorini M., Gaber M., Regni Ponzeveroni R., Sidoli L., & Vercellone S., 2013, *Astronomy and Computing*, 1, 33
- Paizis A., & Sidoli L., 2014, *MNRAS*, 439, 3439
- Paizis A., Fiorini M., Franzetti P., Mereghetti S., Regni Ponzeveroni R., Sidoli L., & Gaber M., 2016, in Proceedings of the 11th INTEGRAL Conference Gamma-Ray Astrophysics in Multi-Wavelength Perspective. 10-14 October 2016 Amsterdam, The Netherlands (INTEGRAL2016). INTEGRAL @ INAF-IASF Milano: from Archives to Science, p. 17
- Reig P., 2011, *A&Sp Sc.*, 332, 1
- Romano P., Bozzo E., Mangano V., Esposito P., Israel G., Tiengo A., Campana S., Ducci L., Ferrigno C., & Kennea J. A., 2015, *A&A*, 576, L4
- Shakura N., Postnov K., Kochetkova A., & Hjalmarsdotter L., 2012, *MNRAS*, 420, 216
- Shakura N., Postnov K., Sidoli L., & Paizis A., 2014, *MNRAS*, 442, 2325
- Sidoli L., Paizis A., Fürst F., Torrejón J. M., Kretschmar P., Bozzo E., & Pottschmidt K., 2015, *MNRAS*, 447, 1299
- Sidoli L., 2017, ArXiv e-prints ([arXiv:1710.03943](https://arxiv.org/abs/1710.03943)), in Proceedings of the XII Multifrequency Behaviour of High Energy Cosmic Sources Workshop. 12-17 June, 2017 Palermo, Italy (MULTIF2017). Published online at <http://pos.sissa.it/cgi-bin/reader/conf.cgi?confid=306>, id.52
- Sidoli L., & Paizis A., 2018, *MNRAS*, 481, 2779
- Stella L., White N. E., & Rosner R., 1986, *ApJ*, 308, 669
- Townsend L. J., Coe M. J., Corbet R. H. D., & Hill A. B., 2011, *MNRAS*, 416, 1556
- Walter R., Lutovinov A. A., Bozzo E., & Tsygankov S. S., 2015, *A&A Rev.*, 23, 2
- Winkler C., Courvoisier T., Di Cocco G., Gehrels N., Giménez A., Grebenev S., Hermsen W., Mas-Hesse J. M., *et al.* 2003, *A&A*, 411, L1
- Winkler C., Diehl R., Ubertini P., & Wilms J., 2011, *Space Science Reviews*, 161, 149

Discussion

CHATY: The distinction made with the Corbet diagram between different HMXBs (Be systems, SgHMXBs and SFXTs) seems not so valid anymore looking at all your plots (SFXTs for instance covering all parameter range).

SIDOLI: Thanks for your comment. Indeed, SFXTs sometimes cover regions typical of both Be/XRBs and SgHMXBs.